Size- and Temperature-Dependent Magnetic Response of Molecular Cage Clusters: Manganese-Doped Tin Clusters

Urban Rohrmann, Sascha Schäfer,[†] and Rolf Schäfer*

Eduard-Zintl-Institut für Anorganische und Physikalische Chemie, Technische Universität Darmstadt, Petersenstrasse 20, 64287 Darmstadt, Germany

Received: June 30, 2009; Revised Manuscript Received: August 31, 2009

Endohedral clusters, formed by incorporating a single Mn atom into a cage of tin atoms, have been generated in the gas phase. Mass spectrometry reveals that a cage size of 10 tin atoms is necessary for the efficient incorporation of one Mn atom. Some of the cluster compounds with one Mn atom attached to the tin clusters display large intensities compared to the pure tin clusters, indicating that the compound clusters are particularly stable. The manganese-doped tin cluster assemblies $Mn@Sn_{12}$, $Mn@Sn_{13}$, and $Mn@Sn_{15}$ have been further analyzed within a molecular beam magnetic deflection experiment. Interestingly, although the effect of the magnetic field on the behavior of $Mn@Sn_{12}$ is quite different from that of $Mn@Sn_{13}$ and $Mn@Sn_{15}$, the magnetic dipole moments are the same within the uncertainty of the measurements. Magnetic dipole moments have been found in close agreement with the spin quantum number $S = {}^5/_2$ predicted by theory for $Mn@Sn_{12}$, indicating that the magnetic moment of the Mn atom is not quenched. This supports the idea that within a tin cluster cage a single Mn atom can be encapsulated, resulting in the formation of endohedral clusters consisting of a central Mn^{2+} ion surrounded by a particularly stable Zintl-ion cage Sn_N^{2-}. The observed molecular beam profiles indicate that at a nozzle temperature of 55 K the magnetic moment is strongly locked to the molecular framework of $Mn@Sn_{12}$; in contrast, the magnetic moment of $Mn@Sn_{13}$ and $Mn@Sn_{15}$ tends to align with the magnetic field. The experiments therefore demonstrate that the size of a presumably nonmagnetic cluster cage might have a fundamental influence on the magnetization dynamics of paramagnetic species. The influence of vibrational excitation on the Stern−Gerlach profile of $Mn@Sn_{12}$ is further analyzed, and it is shown that the behavior of $Mn@Sn_{12}$ at elevated nozzle temperatures changes continuously toward a nonlocked moment, pointing to size- and temperature-dependent magnetization dynamics.

Introduction

Metal-encapsulated clusters of heavy group 14 elements have received much attention very recently, because some of these cluster compounds are particularly stable and therefore suitable for the assembly of larger aggregates.[1–9] From a theoretical point of view, the quasiaromaticity of the Sn_{12}^{2-} and Pb_{12}^{2-} cages and their relationship with the fullerides has been pointed out.[2–4,10,11] Recently, the influence of various dopant atoms on the structure and magnetism of the compound clusters was investigated for several tin cages, and it is predicted theoretically that $Mn@Sn_N$ species are promising candidates for the formation of paramagnetic endohedral cluster compounds.[10,12] An electron transfer from the central manganese atom to the tin cage is expected, resulting in the formation of a central Mn^{2+} ion surrounded by a particularly stable Zintl-ion cage. It is theoretically predicted that the magnetism of the dopant atom is not quenched. Hence a total magnetic moment for the doped cluster with a magnitude of 5.9 μ_B is expected, corresponding to a total spin quantum number $S = {}^5/_2$. Therefore, we have investigated the formation of manganese-doped tin clusters experimentally. The experiments allow us not only to observe which requirements the size of the Sn cages has to meet for the incorporation of one Mn atom, but also to study the magnetism of the doped clusters within a molecular beam magnetic deflection experiment.

Results and Discussion

Mass Spectrometry. In Figure 1 fractions of time-of-flight (TOF) mass spectra of pure and Mn-doped Sn_N clusters ($N = 6-17$) are shown. The Sn_N clusters were generated from a pure tin rod, whereas the Mn-doped Sn_N clusters were formed by laser vaporization of a mixed Mn:Sn target. For the experiments presented here, a target with an atomic Mn:Sn ratio of 5:95 was used. In the photoionization mass spectrum obtained from the vaporization of the Mn:Sn target, additional signals between the mass peaks of the pure tin clusters appear. These signals are due to the formation of compound clusters with one Mn atom attached to the tin clusters Sn_N. In order to highlight the pick-up of a single Mn atom, it is shown in the inset of Figure 1, how the intensity fraction f of the doped tin clusters changes with cluster size N. Even if one has to be very careful in the interpretation of the observed intensities, the experiments indicate undoubtedly that a tin cluster size of 10 atoms is necessary to attach a single Mn atom. The enhanced intensities observed for some of the doped tin clusters $Mn@Sn_N$, even for a target with a large excess of tin, indicate particularly stable manganese-doped tin cluster compounds for $N > 11$. Since the pick up of a single Mn atom requires a minimum size of 10 tin atoms, this leads to the presumption that the Mn atom is not incorporated into the cage of the tin clusters, nor exohedrally attached to the tin clusters, but endohedrally encapsulated,

* To whom correspondence should be addressed. E-mail: schaefer@cluster.pc.chemie.tu-darmstadt.de.

† Present address: Arthur Amos Noyes Laboratory of Chemical Physics, California Institute of Technology, Mail Code 127-72, 1200 East California Boulevard, Pasadena, CA 91125.

10.1021/jp906140b CCC: $40.75
Published on Web 10/07/2009

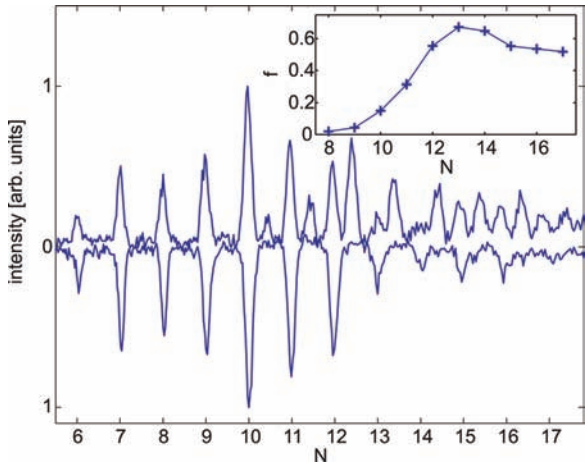

Figure 1. Fraction of time-of-flight mass spectra of pure (lower part) and Mn-doped (upper part) tin clusters. Doped clusters were produced by evaporation of a Mn-doped tin rod (5 at. %). The nozzle temperature of the cluster source was held at 55 K. The formation of singly doped tin clusters is clearly seen. The inset shows the fraction f of Mn-doped species $Mn@Sn_N$, i.e., the intensity i of the species $Mn@Sn_N$ divided by the sum of intensities of the pure and doped species, depending on the number of tin atoms N. The intensity i of a specific cluster size is obtained from the integrated mass peaks.

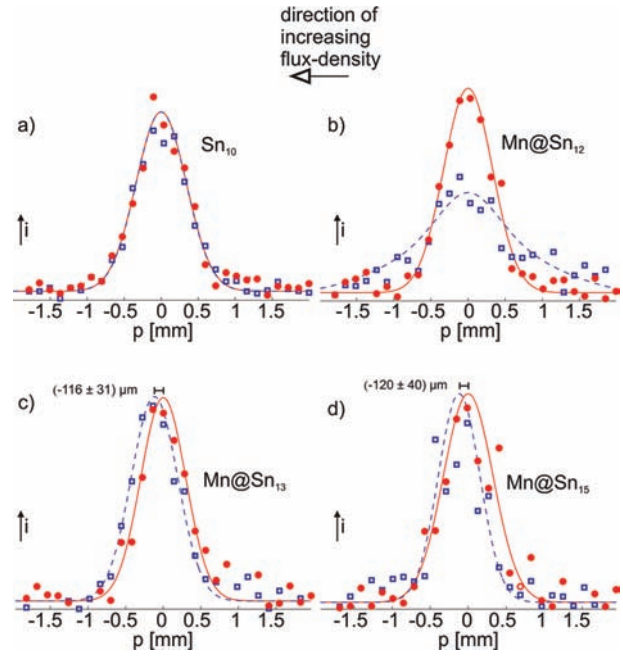

Figure 2. Molecular beam profiles, i.e., the signal intensity i depending on the slit position p, of Sn_{10} (a), $Mn@Sn_{12}$ (b), $Mn@Sn_{13}$ (c), and $Mn@Sn_{15}$ (d), each without (dots) and with (squares) an applied deflection field of 1.6 T at 55 K nozzle temperature. In the case of $Mn@Sn_{12}$ a broadening is observed, indicating a locked magnetic moment, whereas for $Mn@Sn_{13}$ and $Mn@Sn_{15}$ only a net deflection is visible, which corresponds to a Langevin-like behavior. The solid line in each case is obtained by fitting eq 4 to the measured data points without field. The dashed lines in parts a, c, and d are also gaussians fitted to the data points with the magnetic field turned on. In part b the dashed line is derived from eq 3 with a value of $\mu_z = 4.4\ \mu_B$.

because otherwise one would expect that also smaller tin clusters were able to pick up a Mn atom. This idea is strongly supported from quantum chemical investigations of $Mn@Sn_N$.[10] Since according to Wade's Rules,[13] cluster-cages with $2N + 2$ binding electrons can be described as closo-clusters, the donation of two electrons from the dopant-atom leads to the formation of a particularly stable Zintl-ion cluster cage with $2N + 2$ electrons and an additional lone pair on every Sn atom. The doped clusters therefore can be described formally as Zintl-anions Sn_N^{2-} and an endohedrally encapsulated Mn^{2+} cation, whereby the Zintl-ions might form closed polyhedra with triangular faces (deltahedra).[13] The unusual stability of Sn_{12}^{2-} has also been confirmed from mass spectroscopic investigations of $[Al@Sn_{12}]^+$ and photoelectron spectroscopy of $[K@Sn_{12}]^-$[5,7] and $[M@Sn_{12}]^-$ with M = Cu and several other 3d-transition-metals and f-block elements.[12]

Magnetic Deflection Study. ***Experimental Beam Deflection Profiles at $T_{nozzle} = 55$ K.*** In order to corroborate the predicted electronic structures of these compound clusters, we investigated the influence of an inhomogeneous magnetic field on the clusters in the molecular beam and compared the extracted magnetic moments with theoretical predictions.

The dynamics of the magnetic moments of clusters in inhomogeneous fields can be described by two limiting cases: If clusters possess a permanent magnetic moment locked to the molecular framework of the cluster, the magnetic field causes a broadening of the molecular beam,[14] while for clusters that have the moment uncoupled from the geometrical structure spin-relaxation is observed, a phenomenon formally similar to the paramagnetic behavior of isolated spins in condensed phases. The broadening of the molecular beam as a consequence of the magnetic moment may be totally absent if spin-relaxation occurs, but manifests in a deflection of the molecular beam toward high field.[15,16]

These two limiting cases have also been observed for the deflection of particles with an electric dipole moment in an inhomogeneous electric field. While for electric dipole moments it is obvious that the locking of the moment is connected to the rigidity of the clusters' structure and that for floppy clusters the time-averaged permanent dipole moment might vanish,[17] the dynamics of magnetic dipoles is more complicated to understand and still under discussion. For example, excited vibrations have been considered as possible reasons for spin-relaxation as well as avoided crossings of the Zeeman-levels caused by spin-rotation-coupling.[15,16] Whatever might be the reason for spin-relaxation, in an inhomogeneous magnetic field a magnetic dipole moment manifests either in a broadening or a deflection of the molecular beam. In Figure 2 profiles of the molecular beam are presented with and without a magnetic field for $Mn@Sn_N$ clusters with $N = 12, 13, 15$ and as a reference also for Sn_{10}. Since Sn_{10} is predicted to be in a singlet electronic ground-state,[18,19] no effect is expected, which is confirmed by the experiment. In contrast to pure tin clusters, doping with a single Mn atom results in a significant effect. For $Mn@Sn_{12}$ a broadening caused by the magnetic field is observed, while $Mn@Sn_{13}$ and $Mn@Sn_{15}$ are only deflected toward high magnetic field. Both observations point to the presence of a magnetic dipole moment for the manganese-doped clusters. Therefore, it is apparent that the magnetic behavior of the clusters is not only very sensitive to the presence of Mn atoms, but also to the size of the tin cluster cage. The quantitative analysis of the measured molecular beam profiles is still delicate; however, the two limiting cases of locked-spin (a) and paramagnetism (b) are considered here. Obviously, for $Mn@Sn_{12}$ the magnetic dipole moment appears to be locked; on the contrary, the magnetic dipole moment of $Mn@Sn_{13}$ and $Mn@Sn_{15}$ is essentially free to relax in the magnetic field.

(a) $Mn@Sn_{12}$. To discuss the measured beam deflection profiles for locked moments, a perturbation analysis is done, which is valid in the low magnetic field limit. Cui et al. found

for Sn_{12}^{2-} and $Mn^{2+}@Sn_{12}^{2-}$ a ground state structure with icosahedral symmetry (I_h), i.e., a spherical rotor. Assuming the clusters can be treated as rigid, spherical rotors, first order perturbation theory allows us to determine the magnetic moment from the observed beam broadening (adiabatic rotor treatment).[14] The deflection d of a cluster in a given quantum state $|n\rangle$

$$d = -\frac{A}{mv^2} \cdot \frac{\partial B_z}{\partial z} \cdot \mu_z = -\frac{\gamma}{mv^2} \cdot \mu_z \tag{1}$$

then depends on the mass m and velocity v of the cluster, the component of the magnetic moment in field-direction μ_z corresponding to the quantum state $|n\rangle$, and an apparatus constant $\gamma = A \cdot \partial B_z/\partial z$, which is determined by calibration with the Bi atom (see Experimental Section). A in turn is given by the geometry of the apparatus, i.e., the length of the pole-faces and the distance between the magnet and the detector. In order to extract the magnetic moment from the beam profiles, the high temperature limit or weak field approximation is considered. In this case the distribution of the z-component of the magnetic moment, as shown in ref 14, is given by

$$\rho(\mu_z) \approx \frac{1}{2\mu_0} \ln(\mu_0/|\mu_z|) \tag{2}$$

In order to extract the magnitude of the magnetic moment μ_0 from the measured beam profile $\Phi_B(z)$ with the magnetic field applied, one has to convolute $\rho(\mu_z)$ with the molecular beam profile without magnetic field $\Phi_0(z)$

$$\Phi_B(z) = \int \rho(\mu_z) \cdot \Phi_0(d - z) \mathrm{d}\mu_z \tag{3}$$

wherein Φ_0 is given to a very good approximation by a Gaussian

$$\Phi_0(z) = \Phi_0(z = z_0) \cdot \exp\left(-\frac{(z - z_0)^2}{2\sigma^2}\right) \tag{4}$$

Here, $\Phi_0(z = z_0)$ and z_0 represent the height and the location of the maximum and σ^2 is the variance of the beam profile without magnetic field.

Before applying the adiabatic rotor model we must consider the validity of the weak field assumption, i.e., $\mu B_z \ll k_B T_{rot}$. Experimentally, it is found from electric deflection experiments that the rotational temperature for the jet expansion conditions used in the present experiments amounts to a few Kelvin.[20] Considering a magnetic moment of 5 μ_B and a magnetic flux density of 1 T, it is found that $\mu B_z/k_B = 5.5\ \mathrm{K} \approx T_{rot}$. If the condition of weak field is not satisfied, for locked-moments a strong asymmetry of the spatial distribution of the cluster beam is expected[14,21] and indeed a small asymmetry in the measured beam profile is observable by comparing the left and right wings of the deflected profile (see Figure 2b). Even if the weak field assumption is not fully satisfied, from the fact that the beam profiles of $Mn@Sn_{12}$ still show a rather symmetric broadening, it is concluded that eq 3 still is a reasonable assumption to extract the magnitude of the magnetic moment μ_0 of $Mn@Sn_{12}$ from the measured beam profiles. To extract μ_0 from the experimental beam profiles using eqs 2 and 3, the magnitude of the magnetic moment was varied until the root-mean-square deviation between the measured field-broadened beam profile and $\Phi_B(z)$ was minimized. The best fit is obtained for a magnetic moment of (4.4 ± 1.1) μ_B. An additional data set has been analyzed with this procedure, giving a magnetic moment of (6.1 ± 1.5) μ_B, i.e., the mean value of the magnetic moment is given by 5.3 μ_B with a statistical uncertainty of ±1.2 μ_B. Alternatively, it is also possible to extract the magnetic moment from the broadening of the molecular beam, i.e., from the change of the variance σ^2, by fitting Gaussians to the data points with (σ_B^2) and without (σ_0^2) a magnetic field

$$\mu_0 = \frac{3mv^2}{\gamma} \sqrt{\frac{1}{2}\frac{1}{\sigma_0^2} - \frac{1}{\sigma_B^2}} \tag{5}$$

This is done for the data set shown in Figure 2b, and the magnetic moment obtained by this (numerically less consuming) procedure is 3.2 μ_B, indicating that for strong beam broadening this procedure underestimates the magnetic moment, since the beam profile deviates too much from a Gaussian. However, for small broadening this approach is acceptable[20] and the upper bounds for the magnitude of the magnetic moment of the pure tin clusters Sn_{10} obtained by this procedure amounts to $\mu_0 \leq (0.6 \pm 0.6)\ \mu_B$.

(b) Mn@Sn13 and Mn@Sn15. The average magnetic moment $\langle\mu_z\rangle$ of the ensemble of clusters displaying spin-relaxation is determined from the average deflection $\langle d\rangle$ (as calculated from the shift of the maxima of the gaussians applied to the beam profiles with and without magnetic field) via

$$\langle\mu_z\rangle = -\frac{mv^2}{\gamma}\langle d\rangle \tag{6}$$

For an ensemble of clusters possessing spin quantum number S, the magnetic field leads to a splitting into $2S + 1$ magnetic sublevels. However, unlike situations for magnetic atoms (see Experimental Section), the density of (ro)vibrational states in clusters is sufficiently large that transitions between the $2S + 1$ sublevels occur rapidly. If these transitions facilitate a thermal equilibrium among the $2S + 1$ Zeeman sublevels, then the ensemble of clusters will be magnetized with an average magnetic moment $\langle\mu_z\rangle$ as determined by the thermodynamic average of the z-components of the intrinsic magnetic moments

$$\langle\mu_z\rangle = \mu_0 B_S(x) \tag{7}$$

where $B_S(x)$ is the Brillouin function[22] and $x = \mu_0 B_z/(k_B T_{vib})$. Since for the jet expansion conditions used in the present experiments the vibrational temperature of the ensemble of clusters is expected to be close to the nozzle temperature,[23] $x \ll 1$, and for $S \gg 1$ the average magnetic moment in field direction $\langle\mu_z\rangle$ varies quadratically with the magnitude of the magnetic moment (Curie law)

$$\langle\mu_z\rangle = \frac{S+1}{S} \cdot \frac{\mu_0^2}{3k_B T_{vib}} B_z \overset{S\gg1}{\approx} \frac{\mu_0^2}{3k_B T_{vib}} B_z \tag{8}$$

The magnitude of the magnetic moment μ_0 of $Mn@Sn_{13}$ obtained with the Curie law from the data set shown in Figure 2 is (6.7 ± 1.6) μ_B. A second set results in a magnetic moment of (7.6 ± 1.8) μ_B; i.e., the mean value of μ_0 is 7.1 μ_B with a estimated standard deviation of 1.5 μ_B. Interestingly, the

TABLE 1: Experimentally Obtained Magnetic Moments of the Observed Mn-Doped Cluster Species[a]

	$Mn@Sn_{12}$	$Mn@Sn_{13}$	$Mn@Sn_{15}$
$\mu_{0,\,exp}$ [μ_B]	5.3 ± 1.2	6.1 ± 1.3	5.2 ± 2.1
$\mu_{0,\,theo}$[24] [μ_B]	5.9		

[a] For comparison, the value calculated by Kumar et al. for $Mn@Sn_{12}$ is also shown.

magnetic moment of $Mn@Sn_{12}$ is, within the experimental uncertainty, equal to the magnetic moment of $Mn@Sn_{13}$. Actually, the quality of the data sets for the other manganese-doped tin clusters was not good enough to extract magnetic moments for these clusters, $Mn@Sn_{15}$ being the only exception. Here also a deflection of the molecular beam toward high field becomes visible without broadening; i.e., behavior similar to $Mn@Sn_{13}$ is observed. The magnetic moment of $Mn@Sn_{15}$ obtained from two data sets is $(6.2 \pm 2.5)\ \mu_B$.

The observed magnetic moments for $Mn@Sn_N$ with $N = 12, 13, 15$ are close to the value of 5.9 μ_B predicted theoretically for $Mn@Sn_{12}$.[24] This is in accordance with the simple picture, that an electron transfer between the central Mn atom and the tin cluster cage takes place, leaving a high-spin Mn^{2+} ion and a 2-fold negatively charged tin cluster cage. Within this picture the magnetism of the doped cluster is due to the half-filled d-subshell of the central Mn^{2+} ion. For Sn_{12}^{2-} the calculations result in a closed-shell electronic structure;[12] i.e., the electrons have no net orbital angular momentum. Additionally, orbital magnetism is typically quenched for molecules and clusters;[25] i.e., the total angular momentum quantum number J is equal to the spin quantum number S. Therefore, the magnetic moment of the observed clusters belongs to an electronic state with a spin quantum number $S = {}^5/_2$. In the derivation of eq 8 S was approximated to be very large (i.e., S >> 1), which results in the Curie law. With a spin quantum number of $S = J = {}^5/_2$, we correct the magnetic moment, if the values obtained by the Curie law are multiplied by $(S/(S+1))^{1/2}$. The corrected values are shown in Table 1, nicely confirming the magnitude of the magnetic moment $\mu_0 = 2(S(S+1))^{1/2}\ \mu_B = 5.9\ \mu_B$ predicted theoretically.

Spin Dynamics and Response of $Mn@Sn_{12}$ at $T_{nozzle} = 70$, 80, 100 K. Even if the experiments indicate that the picture of spin-only magnetic moment remains valid independent of the tin cluster size, the dynamics of the spin magnetic moments within the magnetic field depends strongly on the size of the tin cluster cage for fixed nozzle temperatures. In order to analyze this, one has to investigate the relaxation of the magnetic moment and the exception of $Mn@Sn_{12}$ in more detail.

The deflection experiment was therefore conducted also at elevated temperatures. Figure 3 shows the beam profiles of $Mn@Sn_{12}$ recorded at nozzle temperatures of 70 K (a), 80 K (b), and 100 K (c). As T_{nozzle} is increased, the intense broadening observed at $T_{nozzle} = 55$ K weakens, at 70 K the measured profile still shows some broadening, but at 80 and 100 K the response is merely given by a deflection toward high-field. The magnetic moment at 100 K can be extracted employing the paramagnetic model, giving $\mu_0 = (6.2 \pm 1.5)\ \mu_B$, in agreement with μ_0 extracted from the broadening at 55 K. Since $T_{vib} \approx T_{nozzle}$, it is concluded that if the vibrational temperatures rises above 70 K, $Mn@Sn_{12}$, formerly showing locked-spin behavior, now displays spin-relaxation. This demonstrates that the degree of thermal excitation is crucial to the paramagnetic behavior of isolated clusters (with only one magnetic atom). But the influence of the thermal excitation on the magnetic moment, giving rise to the temperature- and size-dependent magnetization dynamics, is still unclear.

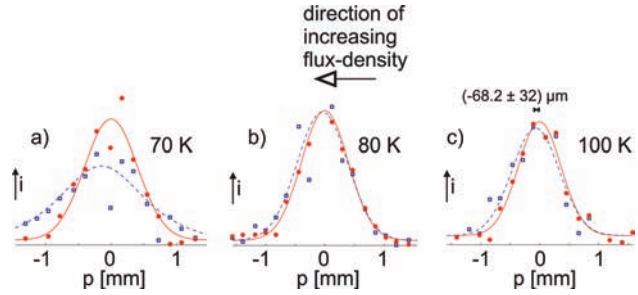

Figure 3. Molecular beam profiles of $Mn@Sn_{12}$ at 70 K (a), 80 K (b), and 100 K (c) nozzle temperature without (dots) and with (squares) an applied magnetic field. As the nozzle temperature is increased to 70 and 80 K, the broadening of the beam (compare with Figure 2b) gets weaker and is almost completely quenched at 100 K, showing merely a deflection of the beam profile without broadening.

The traditional explanation for this spin-relaxation has already been mentioned in the derivation of eq 8; i.e., the Brillouin- and Langevin-function results from the thermodynamic equilibrium of an ensemble of spins with a heat bath, suggesting that the spin thermally relaxes while being in the magnetic field. This implies thermal transitions between magnetic sublevels. However, for the thermal relaxation process to occur in isolated clusters, it is required that the heat bath is internal to the clusters. To be effective, the relaxation time needs to be short compared to the transition time through the magnet (about 100 μs in the present experiment). Therefore a large, thermally excited cluster may serve as a thermal bath for its own spin, particularly if many (ro)vibrational modes are excited. However, as a rule of thumb, if $T_{nozzle} \approx T_{vib} < T_{Debye}/N^{1/3}$,[15] then most of the clusters are vibrationally not excited, and this picture should break down. For α-Sn, T_{Debye} is 200 K,[22] and in the limit of this simple scaling law, the clusters should not be excited very strongly. This discrepancy has led to the suggestion of another mechanism for the alignment of magnetic moments based on an avoided crossing model.[15,16] Here the average magnetic moment $\langle\mu_z\rangle$ results from adiabatic processes of rotating and vibrating clusters in the magnetic field, which gives rise (in the weak field limit) to a Curie-like adiabatic response of the clusters. This is similar to electric deflection experiments, where it has been shown that rotation−vibration couplings, but also external perturbations due to collisions, can strongly influence the measured beam profiles, particularly of asymmetric rotors.[26,27] The external perturbations lead to strongly chaotic behavior of the rotational motion, and in the limiting case the average value of the dipole moment on the axis of the electric field is the same for all molecules of one species and is given by linear response theory.[26] The challenge in applying this approach to the present observation is due to the differences observed for the magnetization dynamics of $Mn@Sn_{12}$ in contrast to $Mn@Sn_{13}$ and $Mn@Sn_{15}$. Therefore, the structures and vibrational spectra were calculated quantum chemically.

Quantum Chemical Study and Discussion

Within the Gaussian03 software package,[28] structure-optimization and harmonic vibrational-frequency analysis for the two species $Mn@Sn_{12}$ and $Mn@Sn_{13}$ were performed. Density functional theory calculations were done employing B3LYP-functionals and Stuttgart−Dresden−ECP and basis set. For Sn atoms only the valence electrons ($5s^2$ and $5p^2$) are considered explicitly, while on Mn the valence electrons ($4s^23d^5$) and one

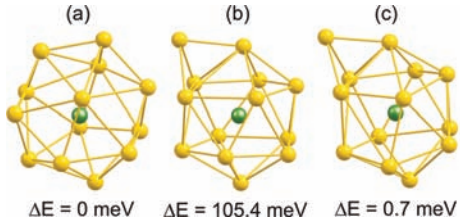

Figure 4. Proposed structures of manganese-doped tin cluster cages with 13 Sn atoms. For $Mn@Sn_{13}$ two (nearly) degenerate structures (a) and (c) were found as minima, and a transition state (b) is shown, connecting these two isomers.

TABLE 2: Lowest Vibrational Modes of $Mn@Sn_{12}$, $Mn@Sn_{13}\{1\}$, and $Mn@Sn_{13}\{2\}$

$Mn@Sn_{12}$ ω [cm^{-1}]	$Mn@Sn_{13}\{1\}$ ω [cm^{-1}]	$Mn@Sn_{13}\{2\}$ ω [cm^{-1}]
53.64	13.58	15.37
53.64	24.08	21.35
53.64	34.06	28.28
53.64	37.99	39.15
53.64	45.60	39.62

shell of inner electrons ($3s^2$ and $3p^6$) are taken into account for the calculations. In accordance with the results of Cui et al.,[6] for the cluster containing 12 Sn atoms and a single Mn atom a structure with icosahedral symmetry is considered and optimized.

For $Mn@Sn_{13}$ we approached the problem of finding the global minimum by using two different starting structures. First, attaching an additional Sn atom above a triangular face of the icosahedron and subsequent optimization results in the structure $Mn@Sn_{13}\{1\}$ (C_s) shown in Figure 4c. In contrast to this, we also used a starting structure corresponding to the proposed structure of the isoelectronic $(BH)_{13}^{2-}$ boranate (C_{2v}),[29] resulting in the structure $Mn@Sn_{13}\{2\}$ (C_{2v}) shown in Figure 4a. This structure can be described as an edge-bridged icosahedron. The two optimized isomers found for the $Mn@Sn_{13}$ cluster show a difference in their zero-point energy of only about 0.7 meV; i.e., the two structures are quasidegenerate at our level of theory. Of course it is not certain that one of these isomers is the true ground-state structure; to stress this, a more thorough search by employing global optimization techniques, e.g., genetic algorithms, would have to be done.

Table 2 shows the lowest vibrational frequencies calculated for $Mn@Sn_{12}$ and $Mn@Sn_{13}$ within the harmonic approximation. The differences in the vibrational spectra show that the species containing 13 tin atoms is strongly excited vibrationally at $T_{vib} = 55$ K, in contrast to $Mn@Sn_{12}$. Therefore, the vibration/rotation coupling in $Mn@Sn_{12}$ might differ substantially from that of $Mn@Sn_{13}$, giving rise to the different spin dynamics observed. Alternatively, the differences observed in spin dynamics of $Mn@Sn_{12}$ and $Mn@Sn_{13}$ might result from an isomerization process. Therefore, a transition state (first order saddle point) was searched with the Gaussians Transit-Guided Quasi-Newton method, connecting the two considered isomers of $Mn@Sn_{13}$. The difference of the zero-point energies of the transition state (see Figure 4) and the ground-state structures is 105.4 meV at the above-mentioned level of theory. The time scale for the isomerization process can be evaluated with Eyring's theory,[30] neglecting differences in the rotational and vibrational partition functions. The first-order rate coefficient is calculated to 1000 s^{-1}, i.e., a time constant of 1 ms, for $T_{vib} = 55$ K. With an average beam velocity of 650 m/s and a pole-face-length of 8 cm the cluster is in the field for about 0.123 ms. For an effective spin-relaxation, the isomerization has to proceed fast, measured on the time scale of the transit through the magnet. Therefore, with the activation energy as found by our calculations, the isomerization is not fast enough, and still a profound broadening would be expected. But if the activation energy is smaller by a factor of only 2, this would speed up the process by a factor of about 10^4, so that it would serve effectively for relaxation. Also, the assumption of $T_{vib} \approx T_{nozzle}$ might not be completely satisfied because of insufficient equilibration in the cooling channel, speeding up the isomerization. However, for $Mn@Sn_{12}$ the situation should be vastly different. Here the energy barrier for isomerization of the icosahedral $Mn@Sn_{12}$ can be expected to be much higher, and therefore, the relaxation should start at even higher temperatures.

Though a different vibrational excitation of $Mn@Sn_{12}$ and $Mn@Sn_{13}$ can be considered as a possible reason for the observed differences in magnetization dynamics, both via isomerization reactions and rotation/vibration coupling, there is an alternative explanation based on the different symmetries of the two clusters. $Mn@Sn_{12}$ possesses icosahedral symmetry and is therefore a spherical rotor, whereas the two proposed isomers of $Mn@Sn_{13}$ with C_{2v}, or C_s, symmetry are asymmetric rotors. An important difference between these rotor types concerns their constants of motion, or, quantum mechanically speaking, their good quantum numbers. A spherical rotor with a locked magnetic moment in a magnetic field can be approximately described by good quantum numbers K and M,[31] which describe the projection of its rotational angular moment onto a body-fixed and laboratory-fixed axis, respectively. If the symmetry of the rotor is lowered to an asymmetric rotor, K is no longer a good quantum number. This leads to a high density of avoided crossings in the stark diagram, which can quench the molecular beam broadening, as it was shown for electric field deflection experiments.[26,27,32,33] From the viewpoint of classical mechanics, however, a quantum system with a high density of avoided crossing corresponds to a classical system with a chaotic dynamics. Qualitatively, it is expected, vide infra, that a chaotic system is more ergodic than a system with some obvious constants of motions. But in the limit of complete ergodicity, the time-average of the magnetic moment $/\mu_z$ equals the ensemble average and is therefore the same for all clusters. Otherwise stated, all clusters undergo the same deflection and no beam broadening is observed.

Until now we have assumed that the orientation of the magnetic moment is locked to the structure of the clusters, which simplifies our treatment to the well-known models in electric field deflection experiments. However, it is known, especially from experiments on small ferromagnetic clusters, that often the spin is almost completely uncoupled from the cluster structure. Indeed, de Heer and co-workers[15,16] can explain the field- and temperature-dependent deflection of small Co_N clusters in a simple model with essentially uncoupled spin and rotation. Only at energy level crossings a small spin−rotation coupling has to be considered, which again leads to a high density of avoided crossing with the same consequences as in the asymmetric rotor case, which was discussed above. The important quantity in their model is the ratio of the interaction energy of the magnetic moment with the external field compared to the rotational energy of the system. At low interaction energy, compared to the rotational energy, i.e., at low field strength or high rotational temperature, almost only a single-sided deflection of the molecular beam is observed, whereas in the case of an interaction energy comparable to the rotational energy, i.e., at low field strength or low temperatures, the molecular beam gets considerably broadened. So this would explain our finding of vanishing beam broadening with increasing temperature in the case of $Mn@Sn_{12}$. However, two points have to be mentioned,

which contradicts this viewpoint for our experiments. First, for $Mn@Sn_{12}$ we observe both a deflection to higher and lower field with almost equal magnitude. In the case of Co_N clusters, only a single-sided deflection toward higher field strength is visible. Second, if we assume that $Mn@Sn_{12}$ and $Mn@Sn_{13}$ have the same magnetic moment and are equally thermalized to a specific rotational temperature, they should show a similar molecular beam deflection, which is not the case. This makes us believe that the mechanism, which controls the magnetization dynamics of small Co_N clusters,[15] is not the important one in the $MnSn_N$ system.

Finally, we want to discuss whether a difference in the magnetic anisotropy energy (MAE) between $Mn@Sn_{12}$ and $Mn@Sn_{13}$ might cause their different deflection behavior. For supported clusters it has been observed that MAE is heavily dependent on the size of the cluster as well as on the structure.[34] Therefore, one might speculate that the magnetic anisotropy energy of $Mn@Sn_{12}$ is much higher than for the other observed species, causing the exceptional behavior of $Mn@Sn_{12}$. However, this is rather unexpected, since transitions to higher degrees of symmetry generally cause MAE to decrease.[35] A point that also causes confusion in this context is how the MAE of an icosahedral cluster can be described. Traditionally, MAE is connected to the zero-field-splitting of electronic states due to electric fields of the coordination sphere.[36] But it can be shown that the icosahedral field causes no splitting of 3d states.[35] So, within an icosahedral cluster in first order there should be hardly any preferred orientation of the spin, and the potential energy barriers in between should not be as high as in the less symmetric structures of the Sn_{13}^{2-} ion ("magnetically soft").

Conclusion

In summary, we were able to show that in order to attach a manganese atom to a neutral tin cluster a critical size of 10 Sn atoms is required. This circumstance was linked to the perception that the doping atom is endohedrally enclosed by the tin cage. The doped clusters $Mn@Sn_N$ with $N = 12, 13, 15$ were additionally investigated by a magnetic deflection experiment and the observed effect of the magnetic field on the spatial distribution was found to be in close agreement with a magnetic dipole moment of 5.9 μ_B as theoretically predicted for $Mn@Sn_{12}$. Though the extracted magnetic moments of all three observed species are equal within the uncertainty of the measurement, their dynamic behavior in the magnetic field is vastly different. This is discussed by regarding differences in the vibrational spectra and isomerization dynamics of these clusters as well as by symmetry considerations.

Experimental Section

Cluster generation, mass spectrometry, and magnetic deflection experiments: Isolated clusters have been generated with a laser vaporization cluster source.[37] For that purpose, either a pure tin rod or doped tin rod with 5 at. % of manganese was used. The plasma, which has been created after the laser ablation, was cooled with an excess of gaseous helium so far that the formation of charged and neutral, pure and Mn-doped, tin clusters starts. Before the cluster−helium mixture is expanded into the high vacuum system through a nozzle, it enters a channel held at a constant temperature ($T_{nozzle} = 55$, 70, 80, and 100 K) in order to increase the sensitivity of the molecular beam magnetic deflection experiment and to reduce the flexibility and vibrational excitation of the clusters. The molecular beam then runs through two skimmers and two collimators before it reaches the magnetic field unit. With the analogue of the "two-wire field" a maximum magnetic flux density of 1.7 T can be achieved. After a second field-free length the clusters become photoionized by a pulse of an excimer laser ($\lambda = 157$ nm) and detected afterward with a time-of-flight (TOF) mass spectrometer. This results in the TOF mass spectra shown in Figure 1. For the magnetic deflection experiments, a small slit is additionally put into the molecular beam in front of the mass spectrometer. Now, depending on the slit position p, the intensity i of the various species was measured in the mass spectrometer with the magnetic field switched off and on. This yields the molecular beam profiles presented in Figures 2 and 3. Magnetic moments are either obtained from the beam broadening in a spherical rigid rotor approximation applying first-order perturbation theory for the Zeeman effect or from the beam deflection with the low-field limit of the Brillouin function, assuming that the vibrational temperature of the clusters is equal to the nozzle temperature.[38,39] To derive absolute values for the magnetic moments, the apparatus has been calibrated with the well-known Landé-factor of the Bi atom,[40] and the velocities of the cluster species were determined. The corresponding beam profiles of an atomic Bi beam are shown in Figure 5.

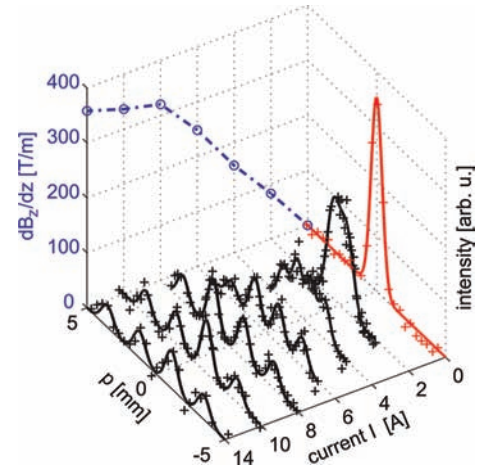

Figure 5. Calibration of the apparatus was done by use of the known Landé-factor of the Bi atom.[40] The figure shows beam profiles of Bi atoms as a function of rising current I. As a magnetic field is applied, the components of the beam with different magnetic quantum numbers m_J clearly separate. In the back on the left (blue circles), the obtained gradient of the magnetic flux density as function of the current is shown. For measurements of paramagnetic species also the magnetic flux density B_z is needed, which was measured with a hall-sensor. For the experiments in this paper, a current of 14 A is used, corresponding to $B_z = 1.63$ T and $\partial B_z/\partial z = 0.358$ T/mm.

The atomic beam is split into four components, resembling the $J = {}^3/_2$ ground state of the Bi atom. The deflection of the different components of the Bi atom together with a measurement of the beam velocity allows for a determination of the gradient of the magnetic flux density. The strength of the magnetic field has been measured with a Hall sensor. The absolute error of the magnetic moments obtained within the rigid rotor approximation is about ±4%, and the magnetic moments calculated from the beam deflection show a systematic error of ±12%. The velocities of the molecular beam were determined by use of a shutter unit with an uncertainty of ±3%. For the errors reported in Table 1 only the uncertainty of the experimental data was taken into account.

Acknowledgment. We acknowledge financial support from the Deutsche Forschungsgemeinschaft by Grant SCHA885/7-2. We also thank Dr. Kathrin Hofmann for her assistance concerning the preparation of the manganese-doped tin targets.

References and Notes

(1) Fässler, T. F.; Hoffmann, S. D. *Angew. Chem., Int. Ed.* **2004**, *43*, 6242.
(2) Chen, Z.; Neukermans, S.; Wang, X.; Janssens, E.; Zhou, Z.; Silverans, R. E.; King, R. B.; von Rague Schleyer, P.; Lievens, P. *J. Am. Chem. Soc.* **2006**, *128*, 12829–12834.
(3) Chen, D.-L.; Tian, W. Q.; Feng, J.-K.; Sun, C.-C. *J. Chem. Phys.* **2006**, *124*, 154313.
(4) Chen, D.-L.; Tian, W. Q.; Feng, J.-K.; Sun, C.-C. *J. Phys. Chem. A* **2007**, *111*, 8277.
(5) Neukermans, S.; Janssens, S.; Chen, Z. F.; Silverans, R. E.; Schleyer, P. v. R.; Lievens, P. *Phys. Rev. Lett.* **2004**, *92*, 163401.
(6) Cui, L.-F.; Huang, X.; Wang, L.-M.; Zubarev, D. Y.; Boldyrev, A. I.; Li, J.; Wang, L.-S. *J. Am. Chem. Soc.* **2006**, *128*, 8390–8391.
(7) Cui, L.-F.; Huang, X.; Wang, L.-M.; Li, J.; Wang, L.-S. *J. Phys. Chem. A* **2006**, *110*, 10169–10172.
(8) Esenturk, E. N.; Fettinger, J.; Lam, Y.-F.; Eichhorn, B. *Angew. Chem.* **2004**, *116*, 2184–2186.
(9) Schäfer, S.; Schäfer, R. *ChemPhysChem* **2008**, *9*, 1925.
(10) Chen, X.; Deng, K.; Liu, Y.; Tang, C.; Yuan, Y.; Tan, X. W. *J. Chem. Phys.* **2008**, *129*, 94301.
(11) Chen, X.; Deng, K.; Liu, Y.; Tang, C.; Yuan, Y.; Hu, F.; Wu, H.; Huang, D.; Tan, W.; Wang, X. *Chem. Phys. Lett.* **2008**, *462*, 275–279.
(12) Cui, L.-F.; Huang, X.; Wang, L.-M.; Li, J.; Wang, L.-S. *Angew. Chem.* **2007**, *119*, 756–759.
(13) Wade, K. *Adv. Inorg. Chem. Radiochem.* **1976**, *18*, 1.
(14) Bertsch, G. F.; Yabana, K. *Phys. Rev. A* **1994**, *49*, 1930.
(15) Xu, X.; Yin, S.; Moro, R.; de Heer, W. A. *Phys. Rev. Lett.* **2005**, *95*, 237209.
(16) Xu, X.; Yin, S.; Moro, R.; de Heer, W. A. *Phys. Rev. B* **2008**, *78*, 054430.
(17) Dugourd, P.; Rayane, R. A. D.; Benichou, E.; Broyer, M. *Phys. Rev. A* **2000**, *62*, 11201.
(18) Schäfer, S.; Assadollahzadeh, B.; Schwerdtfeger, P. *J. Phys. Chem. A* **2008**, *112*, 12312.
(19) Assadollahzadeh, B.; Schäfer, S.; Schwerdtfeger, P. *J. Comput. Chem., Early View* 2009.
(20) Schäfer, S.; Schäfer, R. *Phys. Rev. B* **2008**, *77*, 205211.
(21) Bertsch, G.; Onishi, N.; Yabana, K. *Z. Phys. D* **1995**, *34*, 213.
(22) Kittel, C. *Einführung in die Festkörperphysik, 14. Auflage*; Oldenbourg: München, 2006; p 133.
(23) Collings, B.; Amrein, A. H.; Rayner, D. M.; Hackett, P. A. *J. Chem. Phys.* **1993**, *99*, 4174.
(24) Kumar, V.; Kawazoe, Y. *Appl. Phys. Lett.* **2003**, *83*, 2677–2679.
(25) Gerson, F.; Huber, W. *Electron Spin Resonance Spectroscopy of Organic Radicals*; Wiley-VCH: Weinheim, 2003.
(26) Antoine, R.; Rahim, M. A. E.; Broyer, M.; Rayane, D.; Dugourd, P. *J. Chem. Phys. A* **2005**, *109*, 8507.
(27) Carrera, A.; Mobbili, M.; Moriena, G.; Marceca, E. *Chem. Phys. Lett.* **2008**, *467*, 14.
(28) Frisch, M. J.; et al. *Gaussian 03, Revision B.02*; Gaussian, Inc.: Pittsburgh PA, 2003;.
(29) Brown, L. D.; Lipscomp, W. N. *Inorg. Chem.* **1977**, *16*, 2989.
(30) Laidler, K. *Chemical Kinetics*, 3rd ed.; Harper Collins Publishers Inc.: New York, 1987.
(31) The spin angular momentum can be neglected in our case since it is small compared to the rotational angular momentum.
(32) Antoine, R.; Rahim, M. A. E.; Broyer, M.; Rayane, D.; Dugourd, P. *J. Chem. Phys. A* **2006**, *110*, 10006.
(33) Farley, F. W.; McClelland, G. M. *Science* **1990**, *247*, 1572.
(34) Gambardella, P.; Rusponi, S.; Veronese, M.; Dhesi, S. S.; Grazioli, C.; Dallmeyer, A.; Cabria, I.; Zeller, R.; Dederichs, P. H.; Kern, K.; Carbone, C.; Brune, H. *Science* **2003**, *300*, 1130.
(35) McHenry, M. E.; O'Handley, R. C.; Dmowski, W.; Egami, T. *J. Appl. Phys.* **1987**, *61*, 4232.
(36) van Wüllen, C. *J. Chem. Phys.* **2009**, *130*, 194109.
(37) Schäfer, R.; Woenckhaus, J.; Becker, J. A.; Hensel, F. *Z. Naturforsch., A* **1995**, *50*, 445.
(38) Schäfer, R.; Schlecht, S.; Woenckhaus, J.; Becker, J. A. *Phys. Rev. Lett.* **1996**, *76*, 471.
(39) Schnell, M.; Herwig, C.; Becker, J. A. *Z. Phys. Chem.* **2003**, *217*, 1003.
(40) Title, R. S.; Smith, K. F. *Phil. Mag.* **1960**, *60*, 1281.

JP906140B